10.1007/s12541-010-0004-5

# Position and Orientation Detection of Capsule Endoscopes in Spiral Motion

**Min-Gyu Kim[1], Yeh-Sun Hong[2,#] and Eun-Joo Lim[2]**

1 Robot Research Center, Korea Aerospace University, 100 Hwajeon-dong, Duckyang-gu, Goyang-city, Gyeonggi-do, Korea, 412-791
2 Dept. of Aerospace and Mechanical Engineering, Korea Aerospace University, 100 Hwajeon-dong, Duckyang-gu, Goyang-city, Gyeonggi-do, Korea, 412-791
# Corresponding Author / E-mail: yshong@kau.ac.kr, TEL: +82-2-300-0287, FAX: +82-2-3158-2988

KEYWORDS: Capsule endoscope, Position and orientation detection, Spiral motion, Rotating magnetic field, Permanent magnet

*In this paper, a position and orientation detection method for the capsule endoscopes devised to move through the human digestive organs in spiral motion, is introduced. The capsule is equipped with internal magnets and flexible threads on their outer shell. It is forced to rotate by an external rotating magnetic field that produces a spiral motion. As the external magnetic field is generated by rotating a permanent magnet, the 3-axes Cartesian coordinate position and 3-axes orientation of the capsule endoscopes can be measured by using only 3 hall-effect sensors orthogonally installed inside the capsule. However, in this study, an additional hall-effect sensor is employed along the rotating axis at a symmetrical position inside the capsule body to enhance measurement accuracy. In this way, the largest position detection error appearing along the rotating axis of the permanent magnet could be reduced to less than 15mm, when the relative position of the capsule endoscope to the permanent magnet is changed from 0mm to 50mm in the X-direction, from -50mm to +50mm in the Y-direction and from 200mm to 300mm in the Z-direction. The maximum error of the orientation detection appearing in the pitching direction ranged between -4° and +15°.*

Manuscript received: March 2, 2009 / Accepted: September 10, 2009

**NOMENCLATURE**

$B_m$ = magnetic flux density of permanent magnet
$B_X$, $B_Y$, $B_Z$ = orthogonal components of $B_m$
$B_r$ = residual induction
$\theta$ = rotational angle of permanent magnet
$E$ = error equation for detecting minimum in error contours
$x_p$, $y_p$, $z_p$ = position of capsule endoscope
$\alpha$, $\beta$, $\gamma$ = rotational angles of capsule endoscope
$R_{XYZ}(\gamma, \beta, \alpha)$ = rotation matrix for capsule orientation

## 1. Introduction

A commercial capsule endoscope can transmit video images of the internal walls of a digestive system to a receiver outside the human body while moving by peristalsis. The passively moving capsule endoscope makes it difficult to observe a specific part because of its inability to move or stop intentionally for a prolonged diagnosis. Hence, many research institutions and industries around the world have embarked on the effort to develop active locomotion, of which remotely maneuvering the capsule endoscope using an external magnetic force without any integrated actuators, is one of the locomotive technologies.

Some of the preceding researches that have used magnetic force to move a capsule, have focused on fabricating a spiral shaped structure on the exterior of the capsule and on producing a rotational motion of the capsule endoscope that is equipped with a diametrically magnetized permanent magnet aligning itself with a rotating magnetic field induced by an AC electromagnet.[1-4] In this case, much effort should be applied to implement the AC electromagnet which can arbitrarily change the orientation of the rotating magnetic field projected on the capsule endoscope inside the human body. Therefore, its size must be large enough to surround the human body like an MRI.

In order to produce a desired forward or backward movement of the capsule by spiral motion, it is necessary to know the position

© KSPE and Springer 2010

and orientation of the capsule endoscope, in terms of a reference coordinate system. This can be implemented e.g. by detecting the magnetic field induced by the magnet inside the capsule, where its mathematical model is used to deduce the capsule position from the detector signal. In several research works,[4-8] multiple hall-effect sensors arranged in a 2-D array were used to track 3-D position of a permanent magnet as location marker, which may be applied to detect the capsule position. On the contrary, in another works, an induction coil installed inside the capsule, was used to detect the magnetic field induced by external excitation coils at reference position.[9,10]

In this paper, we discuss the real-time position and orientation detection algorithm for a remote motion control system which employs a rotating permanent magnet instead of a large tri-axial AC electromagnet, in order to reduce the overall cost and improve the manipulability.[11] Since the rotating external permanent magnet outside the human body is located only at a distance of 100mm to 200mm from the capsule, its volume to induce the magnetic torque for rotating the capsule can be significantly reduced. In order to change the location of the external permanent magnet a multi-DOF manipulator is used, where the position data of the capsule must be also provided.

This paper introduces a new position detection algorithm which is specially tailored to measure the position and orientation of the capsule which is simultaneously rotating with an external permanent magnet in order to produce the spiral motion. The capsule is equipped with miniature hall-effect sensors that are orthogonally installed inside the capsule to measure the Cartesian components of the magnetic flux density vector acting on the capsule. Since only four magnetic field sensors are used, as depicted below, the additional power supply and the installation space for the sensors could be resolved without any significant increase in the capsule size. The great advantage is that the position detection system can be easily added on the capsule motion control system employing the rotating permanent magnet.

## 2. Spiral Motion Device and Configuration of the Position Detection System

The rotary motion of the capsule is generated by the attractive and repulsive forces between the magnets inside and outside the capsule as depicted in Fig. 1(a). The blades on the surface depicted in Fig. 1(b) change to threads when the capsule is rotated by the magnetic field. These threads will move the capsule forward due to the thrust produced by spiral motion. Fig. 1(c) shows the capsule endoscope incorporated with an image sensor, wireless transmitter, battery, diametrically magnetized permanent magnets and hall-effect sensor module.

Fig. 1(d) shows the hall-effect sensor module that measures the orthogonal components $B_X$, $B_Y$, $B_Z$ of the magnetic flux density $B_m$ acting on the capsule. In the $X_c$-coordinate, two sensors are installed symmetrically to the $Y_c$-$Z_c$ plane, in order to compensate the offset effect directly. In this way, the position detection errors can be significantly reduced from the results which could be obtained with only one sensor in each coordinate.[12] However, along the $Y_c$- and $Z_c$-coordinates only one sensor each is mounted, at an offset.

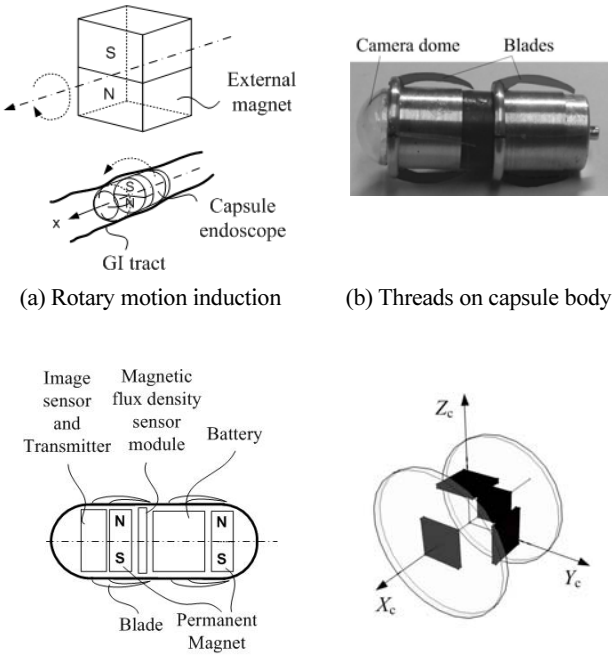


(a) Rotary motion induction (b) Threads on capsule body

(c) Internal components (d) Hall-effect sensor module

Fig. 1 Configuration of capsule position detection system

## 3. Position and Orientation Detection using Hall-Effect Sensors

An induced magnetic flux density or a magnetic field intensity acting on an arbitrary point around a permanent magnet can be mathematically defined. If the magnetic flux density is measured at an arbitrary point where the capsule is, then the relative position and orientation of the capsule from the external permanent magnet can be estimated using the mathematical model of magnetic flux density.

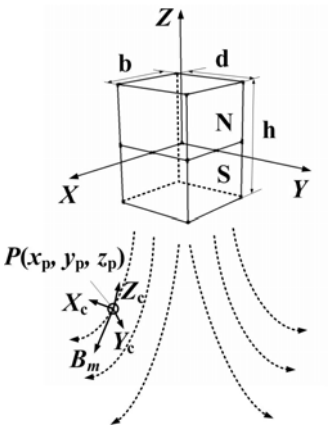


Fig. 2 Flux lines of rectangular parallelepiped permanent magnet

In this study, a rectangular parallelepiped permanent magnet of width b, length d and height h was used as shown in Fig. 2, in order to rotate the capsule and detect its position. At any spatial point $P(x_p, y_p, z_p)$, the magnetic flux density components $B_X$, $B_Y$, $B_Z$ and the scalar magnitude of $B_m$ can be expressed in terms of the size of the permanent magnet, a residual induction and a given position outside the magnet as the following.[13]

$$B_X = \frac{Br}{4\pi}\left[\log\frac{\sqrt{(d-2y_p)^2+(b-2x_p)^2+(h-2z_p)^2}+(d-2y_p)^2}{\sqrt{(d+2y_p)^2+(b-2x_p)^2+(h-2z_p)^2}-(d+2y_p)^2}\right.$$
$$+\log\frac{\sqrt{(d+2y_p)^2+(b+2x_p)^2+(h-2z_p)^2}-(d+2y_p)^2}{\sqrt{(d-2y_p)^2+(b+2x_p)^2+(h-2z_p)^2}+(d-2y_p)^2}$$
$$-\log\frac{\sqrt{(d-2y_p)^2+(b-2x_p)^2+(h+2z_p)^2}+(d-2y_p)^2}{\sqrt{(d+2y_p)^2+(b-2x_p)^2+(h+2z_p)^2}-(d+2y_p)^2}$$
$$\left.-\log\frac{\sqrt{(d+2y_p)^2+(b+2x_p)^2+(h+2z_p)^2}-(d+2y_p)^2}{\sqrt{(d-2y_p)^2+(b+2x_p)^2+(h+2z_p)^2}+(d-2y_p)^2}\right] \quad (1)$$

$$B_Y = \frac{Br}{4\pi}\left[\log\frac{\sqrt{(d-2x_p)^2+(b-2y_p)^2+(h-2z_p)^2}+(d-2x_p)^2}{\sqrt{(d+2x_p)^2+(b-2y_p)^2+(h-2z_p)^2}-(d+2x_p)^2}\right.$$
$$+\log\frac{\sqrt{(d+2x_p)^2+(b+2y_p)^2+(h-2z_p)^2}-(d+2x_p)^2}{\sqrt{(d-2x_p)^2+(b+2y_p)^2+(h-2z_p)^2}+(d-2x_p)^2}$$
$$-\log\frac{\sqrt{(d-2x_p)^2+(b-2y_p)^2+(h+2z_p)^2}+(d-2x_p)^2}{\sqrt{(d+2x_p)^2+(b-2y_p)^2+(h+2z_p)^2}-(d+2x_p)^2}$$
$$\left.-\log\frac{\sqrt{(d+2x_p)^2+(b+2y_p)^2+(h+2z_p)^2}-(d+2x_p)^2}{\sqrt{(d-2x_p)^2+(b+2y_p)^2+(h+2z_p)^2}+(d-2x_p)^2}\right] \quad (2)$$

$$B_Z = \frac{Br}{4\pi}\left[\tan^{-1}\frac{(b-2x_p)(d-2y_p)}{(2z_p-h)\sqrt{(b-2x_p)^2+(d-2y_p)^2+(h-2z_p)^2}}\right.$$
$$+\tan^{-1}\frac{(b+2x_p)(d-2y_p)}{(2z_p-h)\sqrt{(b+2x_p)^2+(d-2y_p)^2+(h-2z_p)^2}}$$
$$+\tan^{-1}\frac{(b-2x_p)(d+2y_p)}{(2z_p-h)\sqrt{(b-2x_p)^2+(d+2y_p)^2+(h-2z_p)^2}}$$
$$+\tan^{-1}\frac{(b+2x_p)(d+2y_p)}{(2z_p-h)\sqrt{(b+2x_p)^2+(d+2y_p)^2+(h-2z_p)^2}}$$
$$-\tan^{-1}\frac{(b-2x_p)(d-2y_p)}{(2z_p-h)\sqrt{(b-2x_p)^2+(d-2y_p)^2+(h+2z_p)^2}}$$
$$-\tan^{-1}\frac{(b+2x_p)(d-2y_p)}{(2z_p-h)\sqrt{(b+2x_p)^2+(d-2y_p)^2+(h+2z_p)^2}}$$
$$-\tan^{-1}\frac{(b-2x_p)(d+2y_p)}{(2z_p-h)\sqrt{(b-2x_p)^2+(d+2y_p)^2+(h+2z_p)^2}}$$
$$\left.-\tan^{-1}\frac{(b+2x_p)(d+2y_p)}{(2z_p-h)\sqrt{(b+2x_p)^2+(d+2y_p)^2+(h+2z_p)^2}}\right] \quad (3)$$

$$B_m = \sqrt{B_X^2+B_Y^2+B_Z^2} \quad (4)$$

If the capsule is in a stationary magnetic field depicted in Fig. 3, its 3-D position data on a toroidal magnetic flux line of constant $B_m$, cannot be determined by measuring $B_m$ only once. Therefore, the magnetic field configuration should be changed to get necessary conditions for solving the above equations. For example, the permanent magnet was translated between two positions in a previous study to get $B_m$ data at different positions of the magnet.[14]

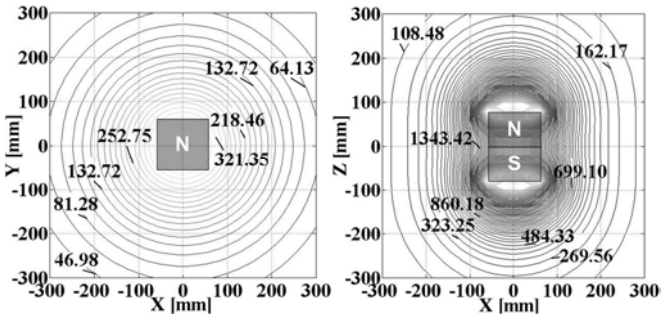


Fig. 3 Equivalent flux density lines of rectangular parallelepiped permanent magnet

In this study, the permanent magnet is rotated along the $X$-axis so that $B_m$ at a particular point is varied periodically, as depicted in Fig. 4(c). $B_m$ reaches its maximum value when the capsule lies in the $X_1$-$Z_1$ plane, and reaches its minimum value in the $X_2$-$Y_2$ plane.

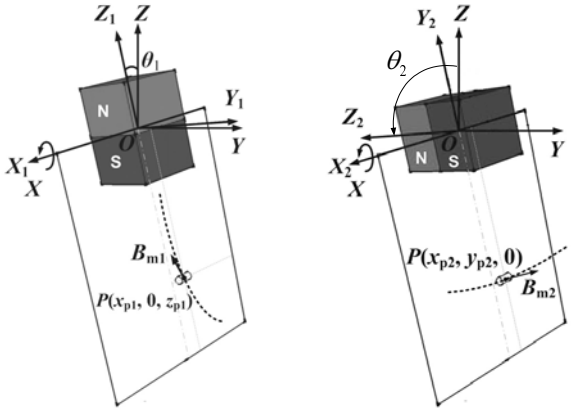


(a) Condition for maximum $B_m$ (b) Condition for minimum $B_m$

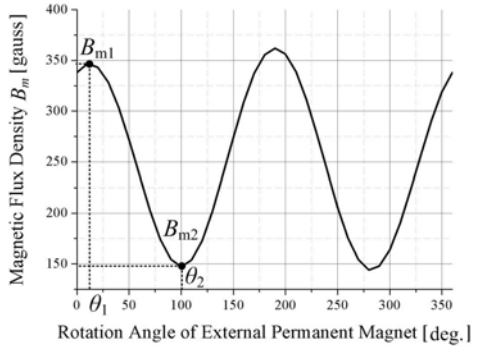


(c) Periodic change of magnetic flux density

Fig. 4 Periodic change of flux density as function of rotation angle

As shown in Fig. 4(a), when the magnetic flux density $B_{m1}$ is maximum value at rotational angle $\theta_1$, the capsule position $y_{p1}$ and

the magnetic flux density $B_{y1}$ on the $Y$-coordinate are zero. The magnetic flux density $B_{m1}$ at $P(x_{p1}, y_{p1}, z_{p1})$ can be represented by substituting $y_{p1} = 0$ in eq. (1)~(4). That is,

$$B_{m1} = \sqrt{B_{x1}(x_{p1},0,z_{p1})^2 + B_{z1}(x_{p1},0,z_{p1})^2} \tag{5}$$

Also, in Fig. 4(b), when the magnetic flux density $B_{m2}$ is minimum value at rotational angle $\theta_2$, the capsule position $z_{p2}$ and the magnetic flux density $B_{z2}$ on the $Z$-coordinate are zero. The magnetic flux density $B_{m2}$ at $P(x_{p2}, y_{p2}, z_{p2})$ can be represented by substituting $z_{p2} = 0$ in eq. (1)~(4). That is,

$$B_{m2} = \sqrt{B_{x2}(x_{p2},y_{p2},0)^2 + B_{y2}(x_{p2},y_{p2},0)^2} \tag{6}$$

$z_{p1}$ in eq. (5) and $y_{p2}$ in eq. (6) are the same magnitude and $x_{p1}$ in eq. (5) and $x_{p2}$ in eq. (6) are the same variables because $X_1$-$Z_1$ plane and $X_2$-$Y_2$ plane are the same, and $\theta_2$ and $\theta_1$ being $\pm 90°$apart. For this reason, the unknowns, $x_{p1}$ and $z_{p1}$, can be obtained using eq. (5) and eq. (6). The $x_{p1}$ and $z_{p1}$ on the $X_1$-$Y_1$-$Z_1$ coordinate are rotated by $\theta_1$ with respect to $X$-axis of $X$-$Y$-$Z$ coordinate. Therefore, the transformation of $x_{p1}$ and $z_{p1}$ into $X$-$Y$-$Z$ coordinate can be expressed as

$$\begin{aligned} x_p &= x_{p1} \\ y_p &= z_{p1}\sin\theta_1 \\ z_p &= z_{p1}\cos\theta_1 \end{aligned} \tag{7}$$

To determine $x_{p1}$ and $z_{p1}$ using eq.s (5) and (6), the error equation is defined as

$$E = \sqrt{((B_{m1})_m - (B_{m1})_c)^2 + ((B_{m2})_m - (B_{m2})_c)^2} \tag{8}$$

where

$(B_{m1})_m$, $(B_{m2})_m$ = measured maximum and minimum magnetic flux density, respectively

$(B_{m1})_c$, $(B_{m2})_c$ = calculated maximum and minimum magnetic flux density, respectively

The orthogonal components of $B_{m1}$ and $B_{m2}$ in eq. (8) can be measured from the hall-effect sensor module. Since the hall-effect sensors cannot be orthogonally mounted at the origin of $X_c$-$Y_c$-$Z_c$ coordinate, they are placed at an offset as shown in Fig. 1(d). In order to irradiate the offset, a hall-effect sensor is placed symmetrically along the $X_c$-axis and the mean value is used. With regard to $Y_c$- and $Z_c$-axis, however, $y_{p1}' = y_{p1} + y_{offset} = y_{offset}$ and $z_{p1}' = z_{p1} + z_{offset}$ are substituted for $y_{p1}$ and $z_{p1}$ in eq. (5) and $y_{p2}' = y_{p2} + y_{offset}$ and $z_{p2}' = z_{p2} + z_{offset} = z_{offset}$ are substituted for $y_{p2}$ and $z_{p2}$ in eq. (6), while calculating $(B_{m1})_c$ and $(B_{m2})_c$ using the mathematical magnetic flux density model. In this research, $y_{offset}$ and $z_{offset}$ are 4mm and 3mm, respectively.

The error contour map expressing eq. (8) in terms of $x_{p1}$ and $z_{p1}$ is shown in Fig. 5. The closed surfaces on the map make sure that any solution converges to a minimum value. In this paper, the Conjugate Gradient Method was applied to find a solution. It is to be noted that the error contour is widened along the $X_{p1}$-axis. For this reason, two hall-effect sensors were used along the $X_c$-axis to

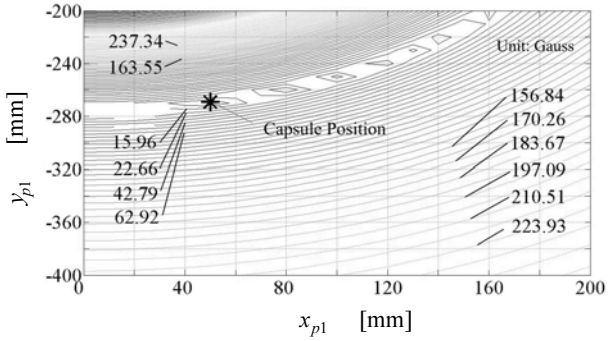


Fig. 5 Error contours

directly detect the magnetic flux density component at the origin of $X_c$-$Y_c$-$Z_c$ coordinate as described above, where the offset effect was canceled by averaging their output signals. As a result, the $x$-position error was reduced compared to the previous research,[11] where only one sensor was used on the $X_c$-axis. However there were no changes in the error reduction in the $y$- and $z$-position errors when two sensors were used along the $Y$- and $Z$-axis respectively.

When the capsule is rotating with respect to the $X$-, $Y$- and $Z$-axis, the orthogonal components, $B_X$, $B_Y$ and $B_Z$ are changing. So the transformation for the capsule orientation can be expressed as shown in eq. (9) using the $X$-$Y$-$Z$ fixed angle.[15]

$$\begin{bmatrix} B_Z' \\ B_Y' \\ B_Z' \end{bmatrix} = R_{XYZ}(\gamma,\beta,\alpha)\begin{bmatrix} B_X \\ B_Y \\ B_Z \end{bmatrix} \tag{9}$$

where $[B_X, B_Y, B_Z]^T$ is the calculated orthogonal components of $B_m$ at the measured capsule position when the rotational angles of the capsule, $\alpha$, $\beta$, $\gamma$ at this position are considered to be zero, $[B_X', B_Y', B_Z']^T$ is the measured orthogonal components from each of the hall-effect sensors while the capsule is being rotated, and $R_{XYZ}(\gamma, \beta, \alpha)$ is the rotation matrix expressed in the $X$-$Y$-$Z$ fixed angle method. The rotation angles $\alpha$, $\beta$, $\gamma$ are shown in Fig. 6.

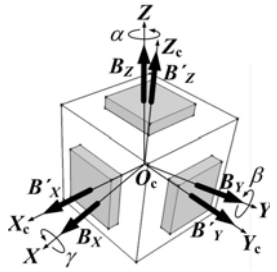


Fig. 6 3-axes rotation expressed by $X$-$Y$-$Z$ fixed angle

## 4. Experimental Setup

The experimental apparatus consists of a magnetic field generating permanent magnet, an electrical motor that rotates the permanent magnet with respect to the $X$-axis and the multi-DOF planar robot that moves the permanent magnet as desired(Fig. 7). The parallelepiped permanent magnet is made of NdFeB with a

residual induction of 1.42T. In order to produce a uniform magnetic field, five rectangular magnets (120×120×30[mm]) and two rectangular magnets (80×80×20[mm]) were separately magnetized and put together as shown in Fig. 8.

The apparatus also consists of a capsule that is specially designed for this experimental purpose, a 3-axis gimbal for holding the capsule, and a computation unit that detects the capsule position from the measured magnetic flux density and the rotation angle of the external permanent magnet. Inside the capsule there were installed a hall-effect sensor module and two disk-type permanent magnets measuring 2mm in thickness and 9mm in the diameter. The hall-effect sensor module consists of four sensors made by Allegro Microsystem, Inc. with a sensing range of ±1200 Gauss(Model no. A1391). Fig. 9 shows the hall-effect sensors mounted on a flexible PCB and the sensor module assembly.

Fig. 10 shows the gimbal that helps the capsule perform a roll motion with fixed pitch and yaw angles at one position under the influence of the rotating external permanent magnet. In the experiment, the gimbal was located at a specific point on the *X*-*Y* plane and the relative position of the external permanent magnet was changed using the manipulator.

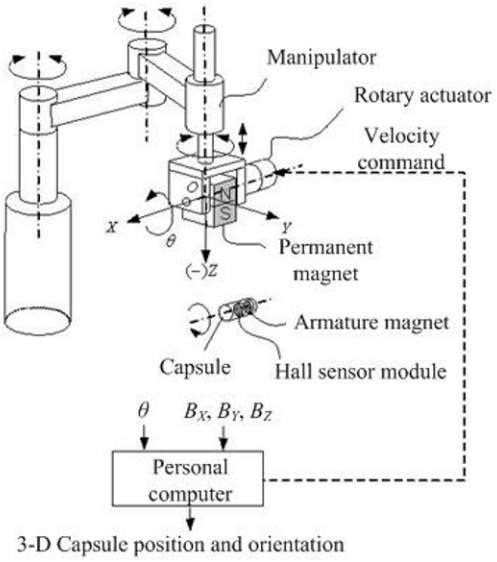


Fig. 7 Experimental setup

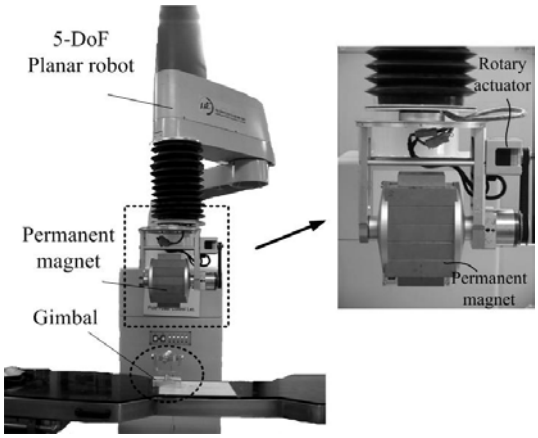


Fig. 8 Permanent magnet and hall-effect sensor module

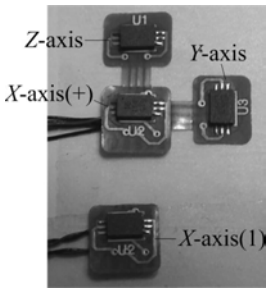


(a) Hall-effect sensors on flexible PCB

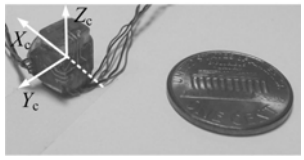


(b) Hall-effect sensor module assembly

Fig. 9 Hall-effect sensor module

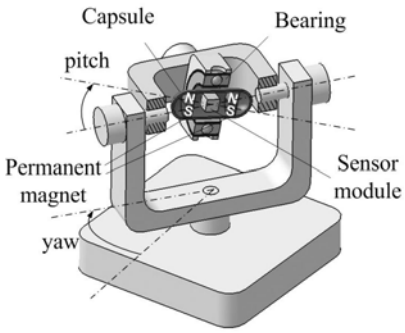


Fig. 10 Capsule body mounted on gimbal

## 5. Experimental Results

The experiment was carried out from 0mm to 50mm in the *X*-direction, from -50mm to +50mm in the *Y*-direction and from 200mm to 300mm in the *Z*-direction. Shown in Fig. 11 is the grid, the points on which the measurements were taken. The capsule was placed on the point 13 as the origin of the coordinates. 10 measurements were taken at each point on the *X*-*Y* grid, at 200, 250 and 300mm along the *Z*-axis, while the permanent magnet was rotated and moved along the gird by the manipulator.

Fig. 12 shows the output signals from the hall-effect sensors when the magnet was at *P*(30,0,250), as an example. $B_X$ and $\hat{B}_X$

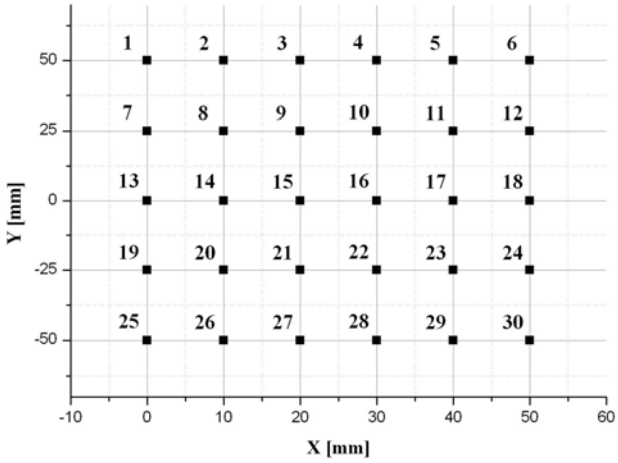


Fig. 11 Target positions for position detection

denote the magnetic flux densities measured by the two sensors that are installed symmetrically to the $Y_c$-$Z_c$ plane, respectively. Because of the offset effect there is a slight difference in their magnitudes. In order to cancel the offset effect directly, their mean value was used in this study, as mentioned above.

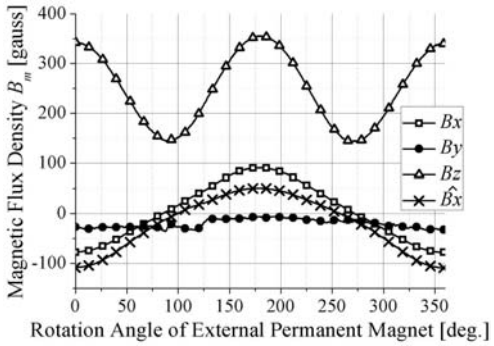


Fig. 12 Output signals from hall-effect sensors

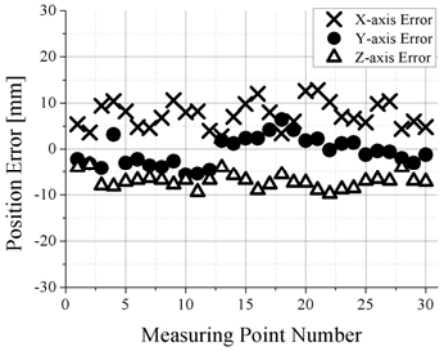


(a) Z=200mm

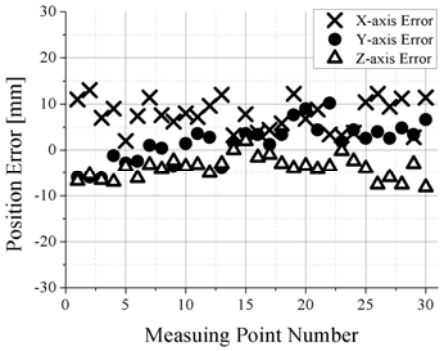


(b) Z=250mm

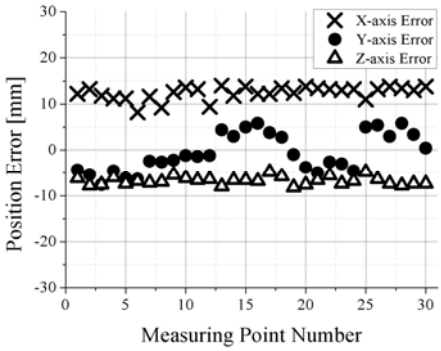


(c) Z=300mm

Fig. 13 Position errors in the *X*-*Y* plane with *Z*-coordinate changed

In Fig. 13, the average *x*-, *y*- and *z*-position error measured at each point in the *X*-*Y* plane are depicted, while *Z*-coordinate was changed. It was observed that the *x*-position error ranged between +2mm and +15mm, the *y*-position error between -9mm and +12mm, and the *z*-position error between -10mm and +3mm. The *x*-position error was greater than the *y*- and *z*-position error because, when the CGM calculates its way towards the real minimum value on the contour map, it is possible that it could converge at point around the real minimum value. As seen in the Fig. 5, the error contours are very broad on the $X_{p1}$-axis.

Fig. 14 shows the repetitive measurements of the capsule orientation, at position *P*(0, 0, 250) with 10°, 20°, 30° pitch angles and 20°, 30° yaw angles. Since the capsule rolls as the permanent magnet rotates, the roll angle has been ignored. The pitch error was between -2° and +13°, and yaw error between -4° and +11°. At different capsule positions the errors did not exceed these ranges.

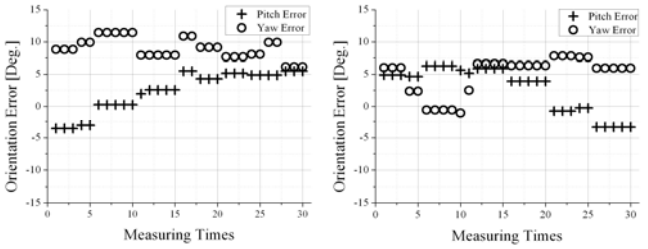


(a) Pitch=10°, Yaw=20° (b) Pitch=10°, Yaw=30°

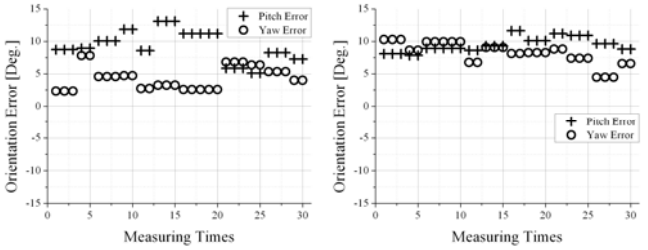


(c) Pitch=20°, Yaw=20° (d) Pitch=20°, Yaw=30°

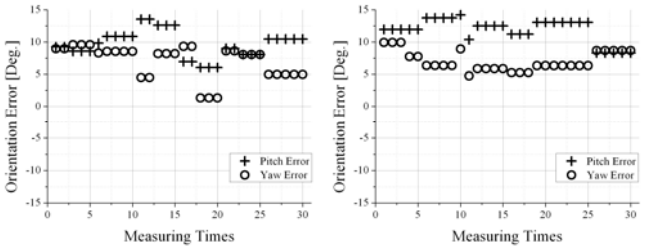


(e) Pitch=30°, Yaw=20° (f) Pitch=30°, Yaw=30°

Fig. 14 Orientation errors with pitch and yaw angles changed

As the experimental conditions are identical when the test was carried out from 0mm to -50mm in the *X*-direction, the above evaluation of the measurement errors can be extended from -50mm to +50mm along with the *X*-coordinate. If we compensate the offsets in the error ranges, the position errors will be less than ±10mm in each coordinate and the orientation errors less than ±8° in the yaw- and pitch direction. Considering the capsule length (25mm), the capsule position error is acceptable. However, the orientation error needs to be reduced in order to precisely detect and manipulate the thrust direction of the spiral motion caused by

rotating capsule. Since the capsule orientation depends on the capsule position, the position error must be further reduced.

In this research, we could confirm the possibility of improving the position and orientation detection accuracy by arranging hall-effect sensors in different configuration.

## 6. Conclusion

This paper presents a position and orientation detection algorithm while the capsule is performing a helical motion in a rotational magnetic flux field. The position and orientation of the capsule can be detected in real-time using four hall-effect sensors inside the capsule. When the relative position of the capsule to the permanent magnet is changed from 0mm and +50mm in the *X*-direction, from -50mm and +50mm in the *Y*-direction and from 200mm and 300mm in the *Z*-direction, the position errors ranged from +2mm to +15mm, from -9mm to +12mm, and from -10mm to +3mm along the *X*-, *Y*-, and *Z*-axis, respectively. The pitch error was between -2° and +13°, and yaw error between -4° and +11°.

The minimum capsule size being 25mm, the maximum position error was acceptable. However, the orientation error should be reduced. In future works, we need to either modify the mathematical model or magnetize the permanent magnet more uniformly so that the deviation of the mathematical model from the actual magnetic field can be reduced.

In addition to it, the proposed position and orientation detection algorithm with hall-effect sensors will be loaded on a wireless capsule and verified in the in-vivo tests.

## ACKNOWLEDGEMENT

This research has been supported by the Intelligent Microsystem Center(IMC; http://www.microsystem.re.kr), which carries out one of the 21st century's Frontier R&D Projects sponsored by the Korea Ministry of Commerce, Industry and Energy and also supported by 2007 Korea Aerospace University Faculty Research Fund.

## REFERENCES

1. Sendoh, M., Ishiyama, K. and Arai, K.-I., "Fabrication of Magnetic Actuator for Use in a Capsule Endoscope," IEEE Trans. on Magnetics, Vol. 39, No. 5, pp. 3232-3234, 2003.
2. Olympus Co., "Medical Device Guidance System," US Patent, No. 20060063974, 2006.
3. Wei, Z., Yingjun, C. and Ping, H., "Study on the System of a Capsule Endoscope Driven by an Outer Rotational Magnetic Field," Proc. of the 2nd Int. Conf. on IEEE/ASME, pp. 1-5, 2006.
4. Dongmei, C., Chao, H., Lei, W. and Max, Q.-H. M., "Active Actuation System of Wireless Capsule Endoscope Based on Magnetic Field," IEEE Int. Conf. on ROBIO, pp. 99-103, 2007.
5. Schlageter, V., Besse, P.-A., Popovic, R. S. and Kucera, P. "Tracking System with Five Degrees of Freedom Using a 2D-Array of Hall Sensors and a Permanent Magnet," Sensors and Actuators A: Physical, Vol. 92, No. 1-3, pp. 37-42, 2001.
6. Prakash, N. M. and Spelman, F. A., "Localization of a Magnetic marker for GI Mobility Studies: An In Vitro Feasibility Study," Proc. of the 19th Int. Conf. of the IEEE EMBS, pp. 2394-2397, 1997.
7. Yabukami, S., Kikuchi, H., Yamaguchi, M., Arai, K. I., Takanishi, K., Itagaki, A. and Wako, N., "Motion Capture System of Magnetic Markers Using Three-Axial Magnetic Field Sensor," IEEE Trans. on Magnetics, Vol. 36, No. 54, pp. 3646-3648, 2000.
8. Wang, X., Meng, M. Q.-H. and Chan, Y., "A Low-Cost Tracking Method Based on Magnetic Marker for Capsule Endoscope," Proc. of 2004 Int. Conf. on Information Acquisition, pp. 524-526, 2004.
9. Nagaoka, T. and Uchiyama, A., "Development of a small wireless position sensors for medical capsule device," Proc. of the 26th Annual Int. Conf. of the IEEE EMBS, pp. 2137-2140, 2004.
10. Eugene, P., Ichiro, S. and Eduard, L., "A New Method for Magnetic Position and Orientation Tracking," IEEE Trans. on Magnetics, Vol. 37, No. 4, pp. 1938-1940, 2001.
11. Lee, J. S., Kim, B. and Hong, Y. S., "A Flexible Chain-based Screw Propeller for Capsule Endoscopes," Int. J. Prec. Eng. Manuf., Vol. 10, No. 4, pp. 27-34, 2009.
12. Kim, M. G., Hong, Y. S. and Kang, H., "Position Detection of Capsule Endoscopes Propelled by Its Spiral Motion," Int. Symp. on Robotics, pp. 216-221, 2008.
13. Furlani, E., "Permanent Magnet and Electromechanical Devices," Academic Press, 2001.
14. Park, J. B., Kang, H. and Hong, Y. S., "Position Detection of a Capsule-Type Endoscope by Magnetic Field Sensors," J. of KSPE, Vol. 24, No. 6, pp. 66-71, 2007.
15. John, J. C., "Introduction to Robotics: Mechanics and Control," Prentice Hall, 2004.